



Universiteit
Leiden
The Netherlands

The quantum dynamics of H₂ on Cu(111) at a surface temperature of 925K: comparing state-of-the-art theory to state-of-the-art experiments
Smits, B.; Somers, M.F.

Citation

Smits, B., & Somers, M. F. (2022). The quantum dynamics of H₂ on Cu(111) at a surface temperature of 925K: comparing state-of-the-art theory to state-of-the-art experiments. *The Journal Of Chemical Physics*. doi:10.1063/5.0112036

Version: Accepted Manuscript

License: [Leiden University Non-exclusive license](#)

Downloaded from: <https://hdl.handle.net/1887/3464641>

Note: To cite this publication please use the final published version (if applicable).

The quantum dynamics of H₂ on Cu(111) at a surface temperature of 925K: comparing state-of-the-art theory to state-of-the-art experiments

Accepted Manuscript: This article has been accepted for publication and undergone full peer review but has not been through the copyediting, typesetting, pagination, and proofreading process, which may lead to differences between this version and the Version of Record.

Cite as: J. Chem. Phys. (in press) (2022); <https://doi.org/10.1063/5.0112036>

Submitted: 20 July 2022 • Accepted: 06 September 2022 • Accepted Manuscript Online: 07 September 2022

 Bauke Smits and Mark F Somers



View Online



Export Citation



CrossMark

ARTICLES YOU MAY BE INTERESTED IN

[NQCDynamics.jl: A Julia package for nonadiabatic quantum classical molecular dynamics in the condensed phase](#)

The Journal of Chemical Physics **156**, 174801 (2022); <https://doi.org/10.1063/5.0089436>

[Relating Dynamic Free Volume to Cooperative Relaxation in a Glass-Forming Polymer Composite](#)

The Journal of Chemical Physics (2022); <https://doi.org/10.1063/5.0114902>

[Electronic Transition of the I-C₆⁺ Cation at 417 nm](#)

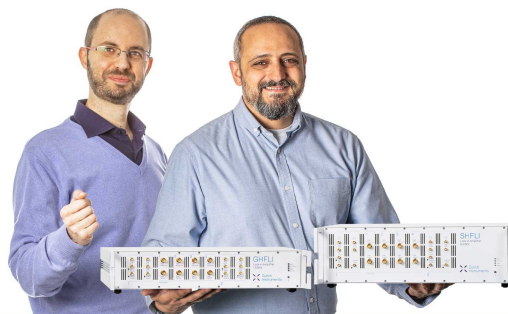
The Journal of Chemical Physics (2022); <https://doi.org/10.1063/5.0106183>

Webinar

Meet the Lock-in Amplifiers
that measure microwaves

Oct. 6th – Register now

 Zurich
Instruments



The quantum dynamics of H₂ on Cu(111) at a surface temperature of 925K: comparing state-of-the-art theory to state-of-the-art experiments

B. Smits and M.F. Somers^{a)}

Leiden Institute of Chemistry, Gorlaeus Building, Leiden University, 2300 RA Leiden, The Netherlands

(Dated: 5 September 2022)

We present results on our recently expanded static corrugation model (SCM) approach to including the relevant surface temperature effects, applied to the dissociative chemisorption reaction of H₂ on a Cu(111). The reaction and rovibrationally elastic scattering probabilities we obtain at a quantum dynamical (QD) level, as an average of many statically distorted surface configurations, show great agreement with those of a dynamic surface model, which reinforces the validity of the sudden approximation inherent to the SCM. We further investigate several simple methods of binning the final rovibrational state of quasi-classical dynamics simulations, to find those best suited to reproduce QD results for our system. Finally, we show that the SCM obtained results reproduce experimental dissociation curves very well, when the uncertainty in experimental saturation values are taken into account. Some indication of a slow channel, so far only observed in experiment, can also be found at low incidence energies, although more rigorous QD simulations are required to reduce the noise inherent to our propagation methods.

I. INTRODUCTION

Heterogeneous catalysis is one of the backbones of modern life, being vital in processes such as steam reforming, for H₂ production, and the Haber-Bosch process, for the production of fertilizer.^{1,2} Here the accurate modelling of gas-surface dissociation reactions is an important topic, as it is often the rate-limiting elementary step in these reactions.³ Past works often relied on simple static and ideal surface models to describe the elementary reactions, neglecting the potentially important effects of energy exchange with the surface or thermal distortion of the surface. As industrial heterogeneous catalysis processes generally take place well above 0K, further gains in the description of these simple dissociation reactions can be attained by finding accurate models for describing surface temperature effects.⁴

For this study, our system of choice is the dissociative chemisorption of H₂ on a (thermally excited) Cu(111) surface. This system is one of the model systems in the field of surface science, with an array of experimental^{5–12} and theoretical^{13–26} data available. In particular, Kaufmann *et al.* recently presented experimental results that allowed them to fully characterise a slow reaction channel for the system, which shows strong temperature and vibrational dependencies, but has not yet been observed in any theoretical works.¹¹ Similarly, Chadwick *et al.* recently published sharply defined state-to-state diffraction probabilities at a surface temperature of 130K, using their molecular interferometry setup.^{12,27}

Several theoretical works have also recently been published, with Dutta *et al.* presenting their work on the effective Hartree potential (EfHP) approach to include surface temperature effects into the H₂ on Cu(111) model at

a quantum dynamical level.^{28,29} Zhu *et al.* demonstrated that an atomistic neural network potential (NNP), with the surface degrees of freedom (DoF) included, can be constructed for several facets of the Cu surface, using only a limited data set.²¹ Smits *et al.* demonstrated surface temperature effects could be accurately included into 6D quantum dynamical (QD) simulations for the rovibrational ground state of H₂ on Cu(111) using the static corrugation model (SCM),²⁶ and at a quasi-classical (QC) level for a range of rovibrational states of D₂ on Cu(111).²³ For other systems, many other approaches for including surface temperature effects have also been suggested, such as the reaction path Hamiltonian (RPH) by Jackson and co-workers,^{30–32} the static disorder parameter by Kroes *et al.*,³³ the reactive force-field (RFF) based approach by Busnengo and co-workers,^{34–36} ring polymer molecular dynamics (RPMD),^{37,38} as well as a variety of high-dimensional NNPs.^{39–41}

For this work, we have chosen to make use of the SCM approach to describe the effect of surface temperature on the H₂/Cu(111) system, as it has been shown to be accurate at both a QC and a QD level for not only dissociation but also rovibrationally elastic scattering probabilities.^{23,26} Our ideal lattice 6D PES of choice was fitted by Nattino *et al.* using the corrugation reducing procedure (CRP),⁴² with a dataset obtained using density function theory (DFT) and the SRP48 functional.⁴³ SRP48 has already shown to reproduce experimental results to within chemical accuracy with the Born-Oppenheimer static surface (BOSS) approach, where the electron and nucleus dynamics are assumed to be fully separable and the surface atoms are kept at their ideal lattice positions.⁴⁴ The SCM then expands on this potential through the addition of a coupling potential, also fit to SRP48 DFT data, which describes the effect of distorting the surface due to thermal effects.¹⁵ Surface configurations are obtained using an embedded atom method (EAM) potential, which has been shown

^{a)} Electronic mail: m.somers@chem.leidenuniv.nl

to accurately reproduce various observables for the copper surface.⁴⁵ Electronic friction due to electron-hole pair excitations has been shown to not be relevant for this system, and is thus not included in this model.⁴⁶

One of the main assumptions of this EAM-SCM approach is that the Cu(111) surface dynamics can be treated at a sudden approximation level, where the surface atoms are not allowed to move. However, the EAM potential can also be used to describe surface motion during dynamics, as the EAM-SCM could be further expanded to the dynamic corrugation model (DCM). Previous work comparing the results obtained with the EAM-SCM and EAM-DCM [for D₂ on Cu(111)] validated the sudden approximation that lies at the base of the SCM, and proved the limited effect energy exchange with the surface has on this system.²³ Recent work has also shown the SCM to hold well when applied to 6D QD simulations with a statically distorted surface, when treating the incoming H₂ at its rovibrational ground state, although there were some clear differences found between the QC and QD results for the rovibrationally elastic scattering probabilities.²⁶

While we will only treat the H₂/Cu(111) system, the EAM-SCM approach is expected to be general enough to be used for the reaction of other diatomic molecules reacting on a transition metal surface. In particular, the model is expected to perform well when energy exchange with the surface plays only a minimal effect, either due to a large mass mismatch between the surface atoms and the reactant, and/or due to short interaction times with the surface. It also relies on the availability of (a dataset of) accurate DFT results that can be used to both construct the BOSS potential energy surface (PES), and fit the required SCM potential to statically include the surface temperature effects. For Cu in particular, previous work has already shown that the SRP48 functional is transferable to other Cu facets, and thus would be an excellent target for future work.^{47,48} The thermally distorted surface configurations needed for the SCM can be obtained from a variety of sources, such as simple force-fields methods, or constructed using, for example, the Debye-Waller factor.¹⁵ For those systems where energy exchange with the surface is important the DCM would be required, which would then also require a potential to accurately describe the motion of the surface atoms. This has, however, only been tested for the H₂ and D₂ on Cu systems so far, and is only computationally viable at a (quasi-)classical level due to the large number of surface DoF involved.²³ Similarly, we expect electronic friction models to be able to expand the EAM-SCM, although this is currently also only possible at a classical dynamics level.^{49–51}

In this work we present dissociation and elastic scattering probabilities of H₂ on a (thermally distorted) Cu(111) surface slab, obtained using the BOSS approach and EAM-SCM approach at a modeled surface temperature of 925K, both using QD and QCD simulations. To complement the results of the previously published rovibra-

tional ground state (of H₂), we now also investigate several initial rovibrationally excited states. Static surface EAM-SCM results are compared to EAM-DCM results where the surface is allowed to move, to further verify the quality of the sudden approximation for this system (which had so far only been shown for the D₂/Cu(111) system). Several rovibrational binning methods are applied to the final classical state of the QCD results, and compared to the exact quantised of the 6D simulations to verify the quality of these binning methods when applied to the H₂/Cu(111) system. Finally, our QD- and QCD-EAM-SCM dissociation probability curves are compared to those obtained from the direct inversion of desorption experiments at the same surface temperature, both at higher incidence energies and at very low reaction probabilities near the curve onset.

II. METHODS

A. Static corrugation model

The SCM was first described by Wijzenbroek and Somers to statically include surface temperature effects as a correction to the perfect lattice BOSS dynamics commonly used.¹⁵ The model applies a correction to the ideal lattice BOSS PES by including two new contributions: a coupling potential V_{coup} , which describes the effect of the distorted surface atoms on the incoming reactant molecule, and a strain potential V_{strain} , which describes the change of potential energy due to the distorted surface atoms interacting with each other. Together with the ideal BOSS PES, these three terms form the full SCM PES, which will describe the potential felt by the reactant due to the thermally distorted surface slab:

$$V_{SCM}(\vec{r}, \vec{q}, \vec{q}^{id}) = V_{BOSS}(\vec{r}^{id}(\vec{r}), \vec{q}^{id}) + V_{coup}(\vec{r}, \vec{q}^{id}, \vec{q}) + V_{strain}(\vec{q}^{id}, \vec{q}) \quad (1)$$

where \vec{r} the positions of all surface atoms, \vec{q}^{id} the ideal lattice positions of all surface atoms and \vec{r} describes the positions of all adsorbed H atoms. $\vec{r}^{id}(\vec{r})$ scales the expanded lattice H₂ coordinates \vec{r} along the c.m. vectors U and V to their ideal lattice coordinates in such a way that they correspond to the same relative coordinates on the surface, as the original BOSS PES is only constructed for r^{id} and the ideal, perfect lattice.¹⁵

As the SCM still relies on a static surface, this description can be further simplified by neglecting the strain potential during dynamics, since the derivative is a constant value. Thus the SCM enables the inclusion of thermal lattice distortions into ideal lattice BOSS dynamics, requiring only an expression for a coupling potential. This coupling potential, in turn, only describes the change in energy of the system due to the reactant atoms interacting with a non-ideal surface. In this, and previous, stud-

ies the form of a switched Rydberg function was chosen for the coupling potential, which is further modified to an effective three-body term by making each of the function parameters (P_{1-7}) linearly dependent on the distance between the two H atoms in the dissociating molecule:²⁰

$$V_{coup}(\vec{r}, \vec{q}^{id}, \vec{q}) = \sum_i^{\vec{r}} \sum_j^{\vec{q}} \left[V_{H-Cu}(|\vec{r}_i - \vec{q}_j|) - V_{H-Cu}(|\vec{r}_i^{id}(\vec{r}) - \vec{q}_j^{id}|) \right] \quad (2)$$

where \vec{r}_i to describe the positions of adsorbate i , \vec{q}_j to describe the surface atom position j . The switched Rydberg-like function is fit to raw DFT data obtained using the same functional as the BOSS CRP potential:¹⁵

$$V_{H-Cu}(R) = (1 - \rho(R))V(R) + \rho(R)V(P_7) \quad (3)$$

with

$$V(R) = -e^{-P_4(R-P_5)} \left(\sum_{k=0}^3 P_k(R-P_5)^k \right) \quad (4)$$

and

$$\rho(R) = \begin{cases} 0 & \text{for } R < P_6 \\ \frac{1}{2} \cos\left(\frac{\pi(R-P_7)}{P_7-P_6}\right) + \frac{1}{2} & \text{for } P_6 \leq R \leq P_7 \\ 1 & \text{for } R > P_7 \end{cases} \quad (5)$$

The distorted surface configurations used are obtained from a previous study of D₂ on Cu(111) where they were generated using molecular dynamics with an embedded atom method (EAM) potential.²³ The EAM potential of choice for the copper surface was published by Sheng *et al.* and has been shown to accurately reproduce a myriad of experimental characteristics, including lattice constant, phonon dispersion curves and thermal expansion coefficients.⁴⁵

By combining this EAM potential with dynamics using the SCM PES, we can go beyond the static surface approximation of the model. Within this dynamic corrugation model (DCM), the energy of the ideal surface is described by a (CRP) PES obtained from DFT, and energy of the Cu surface atoms are described using the accurate EAM potential. The SCM coupling potential is used both to correct the ideal PES for thermal surface distortions, and to describe the effect of the incoming H₂ on the copper surface atoms. Using the DCM, we are able to explicitly include surface motion and energy exchange into our model. A previous study has already shown this addition of surface motion (for the D₂ on Cu(111) system) did not have any significant effect on the reaction or scattering probability for this system.²³

B. Quantum dynamics

To probe the quality of the SCM PES, we perform 6D QD simulations, using the time-dependent wave packet (TDWP) approach to solve the time-dependent Schrödinger equation

$$i\hbar \frac{d\Psi(\vec{Q}; t)}{dt} = \hat{H}(\vec{Q})\Psi(\vec{Q}; t). \quad (6)$$

Here $\vec{Q}(X, Y, Z, r, \theta, \phi)$ is the six-dimensional position vector of the H₂, $\Psi(\vec{Q}; t)$ the time-dependent nuclear wave function of the system, and $\hat{H}(\vec{Q})$ the time-independent Hamiltonian of the system, described as

$$\hat{H}(\vec{Q}) = -\frac{\hbar^2}{2M}\nabla^2 - \frac{\hbar^2}{2\mu r^2}\frac{\partial^2}{\partial r^2} + \frac{1}{2\mu r^2}\hat{J}^2(\theta, \phi) + V(\vec{Q}) \quad (7)$$

with M and μ respectively the mass and reduced mass of the hydrogen molecule, and ∇ and \hat{J} the nabla and angular momentum operators.

The initial wave function $\Psi(\vec{Q}, t = 0)$ is represented as the product of a rovibrational wave function [$\psi_{v,j,m_j}(r, \theta, \phi)$] of the H₂, a two-dimensional plane wave function [$\phi(k_0^X, k_0^Y)$] along X and Y and a Gaussian wave packet [$u(Z; Z_0, k_0^Z)$] centered around a point far away from the surface

$$\Psi(\vec{Q}, t = 0) = \psi_{v,j,m_j}(r, \theta, \phi)\phi(k_0^X, k_0^Y)u(Z; Z_0, k_0^Z) \quad (8)$$

The 6D PES [$V(\vec{Q})$] is obtained from either the BOSS approach and described with the SRP48 CRP PES⁴³ (V_{BOSS}), or from the EAM-SCM approach, where this CRP PES is further expanded with the effective three-body SCM coupling potential (V_{coup}). V_{strain} is ignored in this QD-EAM-SCM work, as the surface quantum dynamics is treated on a sudden approximation level during the, otherwise fully correlated, QD of H₂. This sudden approximation has already been shown to hold for D₂ at a QC level, as well as for the rovibrational ground state of H₂ at a QD level.^{23,26} The dataset of thermally distorted surface configurations is obtained from this same study, and contains a total of 25.000 configurations from 1000 different traces obtained using molecular dynamics with an EAM potential.²³

We propagate our WPs using the split operator (SPO) method⁵²

$$\Psi(\vec{Q}; t_0 + \Delta t) = \exp\left(-\frac{i}{2}K\Delta t\right)\exp(-iV(\vec{Q})\Delta t) \exp\left(-\frac{i}{2}K\Delta t\right)\Psi(\vec{Q}; t_0) + O[(\Delta t)^3] \quad (9)$$

with K the kinetic energy part of our Hamiltonian, as implemented in our in-house code.⁵³ Here the WPs are propagated in a stepwise fashion, first taking a half-step for the free particle propagation, then a full action of the potential is applied, followed by another half-step as a

free particle. This stepwise propagation method inherently results in an error $O[(\Delta t)^3]$ which scales with the size of the time-step used.

A quadratic form of the optical potentials in the scattering and adsorption regions is used,⁵⁴ while the scattered fraction is analysed through the scattering matrix formalism⁵⁵ which yields the scattering probabilities for each rovibrational state and diffraction channel separately. The sticking probability is subsequently calculated by subtracting the sum of all these scattering probabilities from the total possible probability of one. In contrast to the direct flux methods employed in other works,^{41,56} the scattering amplitude method allows us to directly extract diffraction probabilities and rovibrationally resolved scattering results. Particularly rovibrationally resolved scattering probabilities have already been shown to demonstrate larger QD effects when compared to the non-quantised quasi-classical results for the $\text{H}_2/\text{Cu}(111)$ system, and are thus an important part of this work.²⁶ For a more in-depth discussion of the basis of these quantum mechanical methods, we direct the reader to Refs. 57 and 53.

To obtain a single representative dissociation or scattering curve for H_2 reacting with thermally distorted $\text{Cu}(111)$ at a QD level, we average the probabilities obtained for a total of 104 unique thermally distorted surface slabs. By averaging over the results obtained from these thermally distorted surface slabs, the quantum dynamics of the surface atom degrees of freedom is effectively done on a sudden approximation level using Monte-Carlo sampling. Thus we essentially perform QD implicitly even for the surface degrees of freedom, but with the approximation that energy exchange between H_2 and the surface is not possible. Furthermore, there is also no energy exchange possible between the vibrations within the solid during the individual QD TDWP runs, making sure that any classical redistribution or leaking of zero point energy is not possible at all. This is where we think the SCM shines compared to other models, employing thermostats and/or other RPMD assumptions (i.e. using Boltzmann statistics and harmonic potentials) especially relevant for $T_s < 300\text{K}$ for Cu.

For each individual surface configuration, the QD reaction or elastic scattering curve is obtained via three different WPs, one with an energy range from 0.10 eV to 0.30 eV, an other 0.25 eV to 0.70 eV, and a third from 0.65 eV to 1.00 eV, as already used in a previous work for the rovibrational ground state. For the initial rotationally excited states only those states with $mJ \geq 0$ were considered, with the results for $mJ \neq 0$ counted twice in the total average per rotational state, to account for the $mJ < 0$ states. Details regarding the computational parameters for each of these wave packets can be found in the supplementary material.

C. Quasi-classical dynamics

These QD results are compared to results obtained using the quasi-classical (QC) trajectory approach, both using the BOSS PES and the SCM to model a surface temperature of 925K. Furthermore, using the DCM we are able to directly implement surface motion and energy exchange between the reacting H_2 and the Cu surface. For the SCM and BOSS results, a total of 50.000 trajectories were performed for each incidence energy, while for the DCM results at least 1000 trajectories were performed for each incidence energy.

To initiate the QC trajectories, the c.m. of the incoming H_2 is set 7 Å above the surface in the Z direction, and randomly above the surface between 0 and a in the U(= $X - Y/\sqrt{3}$) and V(= $2Y/\sqrt{3}$) directions, with a the lattice constant of our (thermally expanded) surface slab. The molecular angles θ and ϕ are randomly chosen from a uniform distribution on the sphere, with $\cos(\theta)$ from -1 to 1 and ϕ from 0 to 2π , respectively. Surface atom displacements for the EAM-SCM and EAM-DCM approaches are randomly selected from the same dataset of 25.000 surface configurations as used in the QD. For DCM, each of these surface configurations also includes a matching set of initial momenta, to ensure the surface remains at the target temperature of 925K. Only those surface atoms within an SCM cutoff distance of 16 bohrs of the unit cell corner (U,V,Z)=(0,0,0) and within the top two layers were included for calculating the SCM coupling potential, as was done in all previous works.^{23,26}

The model is expanded from a classical to a quasi-classical level through the addition of a zero point energy of the initial rovibrational state, which is calculated using the Fourier grid Hamiltonian method.⁵⁸ A constant time-step propagation for one full vibrational cycle is then performed for the H_2 , which yields the quasi-classical distribution of the H–H distances and corresponding momenta. Internal angular velocities are chosen according to the quantized angular momentum $L^2 = J(J+1)\hbar^2$, while the angle θ_L between the angular momentum vector and the surface normal is chosen randomly but constrained by $\theta_L = \pi$ for $J = 0$ and $\cos(\theta_L) = m_j/\sqrt{J(J+1)}$ if $J \neq 0$. The rotational mJ states are chosen equally between $-J$ and J , with the number of trajectories increased to ensure each mJ state has the same number of occurrences. This addition of an initial quantised energy state of the H_2 to the classical dynamics has been shown to be important to accurately reproduce dissociation for the H_2/metal system.⁵³

Then the H_2 molecules are propagated in the micro-canonical ensemble using the PES at a classical level with the Bulirsch-Stoer predictor-corrector algorithm,⁵⁹ according to Hamilton’s equations of motion using the simple Hamiltonian

$$H = \sum_{i=0}^n \left[\frac{p_i^2}{2m_i} \right] + V[R(t)] \quad (10)$$

where p_i and m_i are respectively the momentum and mass of the i th atom and $V[R(t)]$ describes the total potential energy of all n atoms at positions R and time t . Propagation ends when the two H atoms move more than 2.25 Å apart for a reactive trajectory, or when the Z c.m. coordinate is further than 7 Å from the surface for a scattered trajectory.

The final rovibrational state of those H₂ molecules that are scattered is determined using several simple binning methods. First the modulus of the classical angular momentum ($|L_f|$) is calculated

$$|L_f|^2 = p_\theta^2 + \frac{p_\phi^2}{\sin^2 \theta} \quad (11)$$

where p_θ and p_ϕ describe the conjugate momenta along the two molecular angles. This angular momentum is then used to determine a classical 'rotational state'

$$J_{classical} = \frac{\sqrt{1 + 4|L_f|^2} - 1}{2} \quad (12)$$

which is found by equating $|L_f|^2$ to $J(J+1)$.

Next this classical state is binned using one of three methods. Using the standard binning method, which is how we have performed the binning in previous studies, the rotational state is binned to the closest allowed J state, keeping in mind the selection rule for the rotational state of our diatomic molecule: $\Delta J = \pm 2$. With the weighted binning method, the integer rotational state closest to $J_{classical}$ is chosen, and given a weight of $W_i = 2$ when it is allowed, or $W_i = 0$ when it is not allowed, with i for the i th trajectory performed, effectively ignoring any trajectory with a disallowed transition.⁶⁰ Assuming an equal distribution over all the possible classical rotational energies, this would yield an average total weight equal to the number of trajectories performed. Finally, with the floor binning method the classical rotational state $J_{classical}$ is rounded downwards towards the first allowed J state, keeping in mind the selection rule. For both the standard and floor binning, $W_i = 1$ is always chosen for every trajectory.

With the rotational state (J) determined, the vibrational state (v) is chosen by finding the rovibrational state which is closest in total rovibrational energy to the states allowed by the binned rotational state. Trajectories are considered rovibrationally elastically scattered when the final rovibrational state of H₂ is binned to the same state as its initial state, and rovibrationally inelastically when the binned final state is not the same as the initial rovibrational state. The m_J state is not taken into account at all for the final state, as it is degenerate with the other possible m_J states.

Reaction and scattering probabilities are determined by

$$P = \frac{\sum_{reacted} W}{\sum_{total} W} \quad (13)$$

with W being the weight of each individual trajectory. For the standard and floor binning methods, these probabilities are equal to dividing the number of reacted or scattered trajectories by the total number of trajectories performed.

D. Comparisons to experiment

We will also compare our theoretical dissociation curves to those reported in several experimental studies.^{7,8,11} The experimental results we discuss are all obtained from direct inversion of time of flight (ToF) results obtained from desorption experiments. This inverted data is then fitted to a functional form, which range from very simplistic to quite advanced. Here we will only concern ourselves with the very simple error function

$$S(v, J, T_s, E_{kin}) = \frac{A(v, J)}{2} \left[1 + \operatorname{erf} \left(\frac{E_{kin} - E_0(v, J)}{W(v, J)} \right) \right] \quad (14)$$

where the three fitted variables A , E_0 and W are the saturation value, inflection point and width respectively. While absolute E_0 and W parameters can be directly obtained from these inverted ToF spectra, the same can not be said for the saturation value, where only relative values can be found directly. Thus experimental studies often fit their curves under the assumption of a saturation value of $A = 1$, while both experimental and theoretical studies rarely ever find such a value. Furthermore, care should be taken when scaling the curves to different saturation values, as some previous studies have found these three parameters to not be entirely independent. Both references 7 and 11 have also used beam adsorption experiments to determine absolute saturation values for their surfaces. It is, however, unclear if these can be directly applied to their experimental desorption data, due to differences in experimental setup, including surface temperature.

Finally, Kaufmann *et al.* also identified a slow reaction channel, which was fit separately using

$$S_{slow}(v, J, E_{kin}) = A_{slow}(v, J) \exp \left(\frac{-E_{kin}}{\gamma(v, J)} \right) \quad (15)$$

where A_{slow} defines the amplitude, and γ a decay parameter.¹¹ The older works by Rettner *et al.*⁷ and Hodgson *et al.*,⁸ as well as all theoretical works to date, did not find this separate channel.

III. RESULTS AND DISCUSSION

A. Rovibrationally excited states and a dynamic surface

First we will compare the reaction probability curves obtained for both the EAM-SCM and EAM-DCM at a

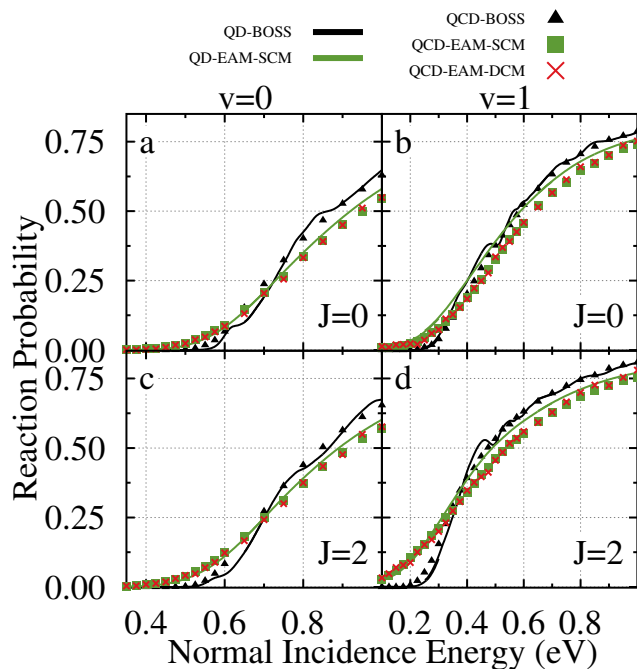


FIG. 1. Reaction probabilities obtained for four initial rovibrational states of H_2 on $\text{Cu}(111)$: (a) $v=0$, $J=0$; (b) $v=1$, $J=0$; (c) $v=0$, $J=2$; (d) $v=1$, $J=2$. Included are the QD- and QCD-EAM-SCM results as a green curve and green squares respectively, QCD-EAM-DCM results as red crosses, and QD- and QCD-BOSS results as a black curve and black triangles respectively. A modeled surface temperature of 925K was used for the SCM and DCM.

QC level to those obtained using QD-EAM-SCM. Previous work has already shown the QD- and QCD-EAM-SCM results show excellent agreement for the rovibrational ground state of H_2 ,²⁶ however, this has not yet been verified for the rovibrationally excited states or when also considering the moving surface of the EAM-DCM, as previous comparisons between QCD-EAM-SCM and -DCM were only performed for the D_2 scattering reaction.²³ In Figure 1, we show some of the reaction probabilities previously obtained for the rovibrational ground state (a), as well as a rotationally excited initial state [(c), v , $J=0$, 2]. Similarly for (b) and (d) we show the results obtained for the vibrationally excited ($v=1$) state, for $J=0$ and $J=2$ respectively. Next to the QCD- and QD-EAM-SCM results, we also included the QCD- and QD-BOSS results, as well as the QCD-EAM-DCM results.

As expected the agreement between QCD and QD, both for the BOSS and EAM-SCM results, is very good, with some minor differences in curve width more prominently visible for the vibrationally excited states. The small fluctuations in the SRP48 CRP PES are much more clearly visible for the QD-BOSS results, compared to the QD-EAM-SCM, primarily due to the averaging over many surfaces we perform to obtain accurate surface temperature effects, as these will smooth out these smaller

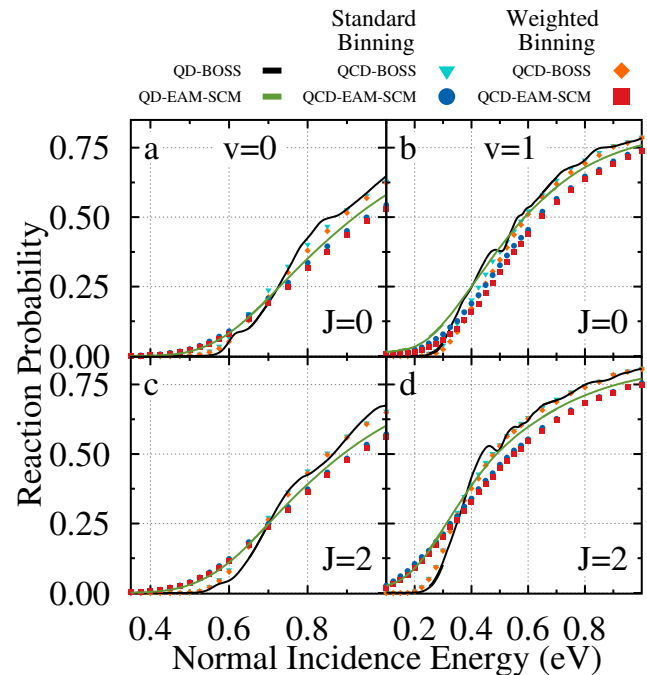


FIG. 2. Reaction probabilities obtained for four initial rovibrational states of H_2 on $\text{Cu}(111)$: (a) $v=0$, $J=0$; (b) $v=1$, $J=0$; (c) $v=0$, $J=2$; (d) $v=1$, $J=2$. The QD results for the BOSS and EAM-SCM results are shown as a black and green curve respectively, while the QCD-BOSS results are displayed as cyan triangles for the standard binning and orange diamonds for weighted binning. The QCD-EAM-SCM results show as blue circles for standard binning, and red squares for weighted binning. A modeled surface temperature of 925K was used for the SCM and DCM.

inconsistencies in the results. The agreement between the QCD-EAM-SCM and -DCM (and thus also with the QD-EAM-SCM) results is again excellent, as was already shown for the $\text{D}_2/\text{Cu}(111)$ system. This observation is perhaps not too surprising, as the mass mismatch between H_2 and the Cu surface is even bigger than that of D_2 and Cu, but it once again confirms the validity of the sudden approximation for this system, and demonstrates the (lack of) effect of energy exchange for the dissociation reaction.

B. Binning methods explored

To achieve the best agreement between QCD and QD results, we also compare three (relatively simple) binning methods to obtain the final rovibrational state of our QCD simulations. This is especially valuable not just for this work, but also for future studies, as finding which QCD binning method compares best compared to rigorous QD simulations will be very important when comparing rovibrationally (in)elastic scattering probabilities. We show the effects of these binning methods on the final dissociation probabilities we compute in Figure 2.,

again for (a) the rovibrational ground state, (b) a vibrationally excited state, (c) a rotationally excited state, (d) and a rovibrationally excited state. As only the weighted binning will have an effect on the final reaction probabilities compared to the standard and floor binning, we have not included the floor binning in this figure. We include binned QCD results obtained with both the BOSS and EAM-SCM PES, as well as QD results from those PESs as a comparison.

We find the same trend for all four rovibrational states, with the standard binning method resulting in slightly higher reaction probabilities compared to the weighted binning. This effect is most noticeable for the $J=0$ states, where the reaction is up to 3 percentpoint higher when using the standard binning method, which could be explained by the lack of lower energy rovibrational states to scatter into compared to the $J=2$ states. In general, these slightly higher probabilities found using standard binning improves agreement with the QD results, both for BOSS and for EAM-SCM, although this effect is small enough that it will not significantly affect any conclusions made using either method.

The same can not really be said when considering the rovibrationally elastic scattering curves for the three binning methods we have included. Figure 3 and 4 present these scattering probabilities for the vibrational ground and first excited state respectively, split for the standard (a,d,g), weighted (b,e,h), and floor (c,f,i) binning methods. Again we take into account the rotational ground state (a-c; $J=0$), but now two additional excited states: (d-f) $J=1$, and (g-i) $J=2$. Next to the binned QCD-EAM-SCM and QCD-BOSS results, we also included the binned QCD-EAM-DCM results. QD-BOSS and -EAM-SCM results are again included as a comparison.

As noted before, the agreement between the QCD-EAM-DCM and QCD-EAM-SCM results is again excellent regardless of the binning method chosen. This matches the findings of earlier work for D_2 on Cu(111), and further shows its independence of the binning method used.

The floor binning method heavily overestimates the elastic scattering probabilities at lower incidence energies compared to the QD results, or underestimates when the initial state is not the lowest allowed rotational state available. Interestingly this also applies for the vibrationally excited states, suggesting that there is little conversion of vibrational to rotational energy, at least at the QCD level. At high incidence energies the agreement with the QD results does appear to be relatively good, although we do not think this binning method is, in general, a good choice for comparisons to QD results.

We find that the standard binning method generally predicts lower scattering probabilities compared to the weighted binning, which can be partially explained by the slightly higher reaction probabilities found for standard binning. Furthermore, those trajectories that are found with a 'classical rotational state' slightly above the first rotational state of the incoming molecule ($\Delta J = +1$) are

often binned 'upwards' to the first allowed state when using standard binning, while these states are completely disregarded for weighted binning. This effect would result in higher probabilities for the lower rotational states when dealing with lower incidence energies, as their energy would not be high enough to 'push' the scattered molecules all the way to the next allowed state. We expect this effect to be especially strong for those states where the lowest allowed rotational state is also the initial state, in our results $J=0$ and $J=1$, and to be much more important for the scattering results, compared to the dissociation probabilities. However, it appears to only be clearly noticeable for the rovibrational ground state, where there is no vibrational energy to convert to higher rotational states, and be somewhat important for the $v=1$, $J=0$ state. Neither of the $J=1$ states show any significant difference we can ascribe to this binning effect.

In general, the QCD binning method that leads to the best agreement with the QD results appears to heavily depend on the initial rovibrational state of the H_2 . The standard binning performs somewhat better than the weighted binning for the $v=0$ states and the $v=1$, $J=0$ state, while the weighted binning method performs a bit better for the $v=1$, $J=1,2$ states, although not by much. The standard binning method underestimates the elastic scattering probabilities for the $v=1$ states primarily at the lower incidence energies, where reaction is also lower, whereas the weighted binning overestimates the $v=1$, $J=0$ probabilities much more over the entire energy range yet shows almost perfect agreement for the rotationally excited states.

For our further comparisons to experimental work, the QCD results we present will be obtained using the standard binning method, as it is the method used in our previous studies. However, future work could focus on applying more complicated Gaussian binning methods, which have shown to improve agreement with QD results when properly used.^{60,61}

C. Comparisons to experiment

Having chosen a binning method that yields QCD results that accurately reproduce our QD curves, we next aim to further validate the (QD-)EAM-SCM approach by comparing our reaction probability curves to those obtained in experimental studies. The three studies we compare to, published by Rettner *et al.*,⁷ Hodgson *et al.*⁸ and Kaufmann *et al.*,¹¹ all obtained their results from desorption experiments, from direct inversion of their ToF results under the assumption of detailed balance.

As we discuss in section IID, this allows these studies to fit absolute values of the width parameter (W) and the inflection point (E_0) as described in equation 14. However, only relative saturation values (A) can be obtained from these experiments. Several approaches were suggested to obtain saturation values that allow for an accurate comparison to our theoretical results.

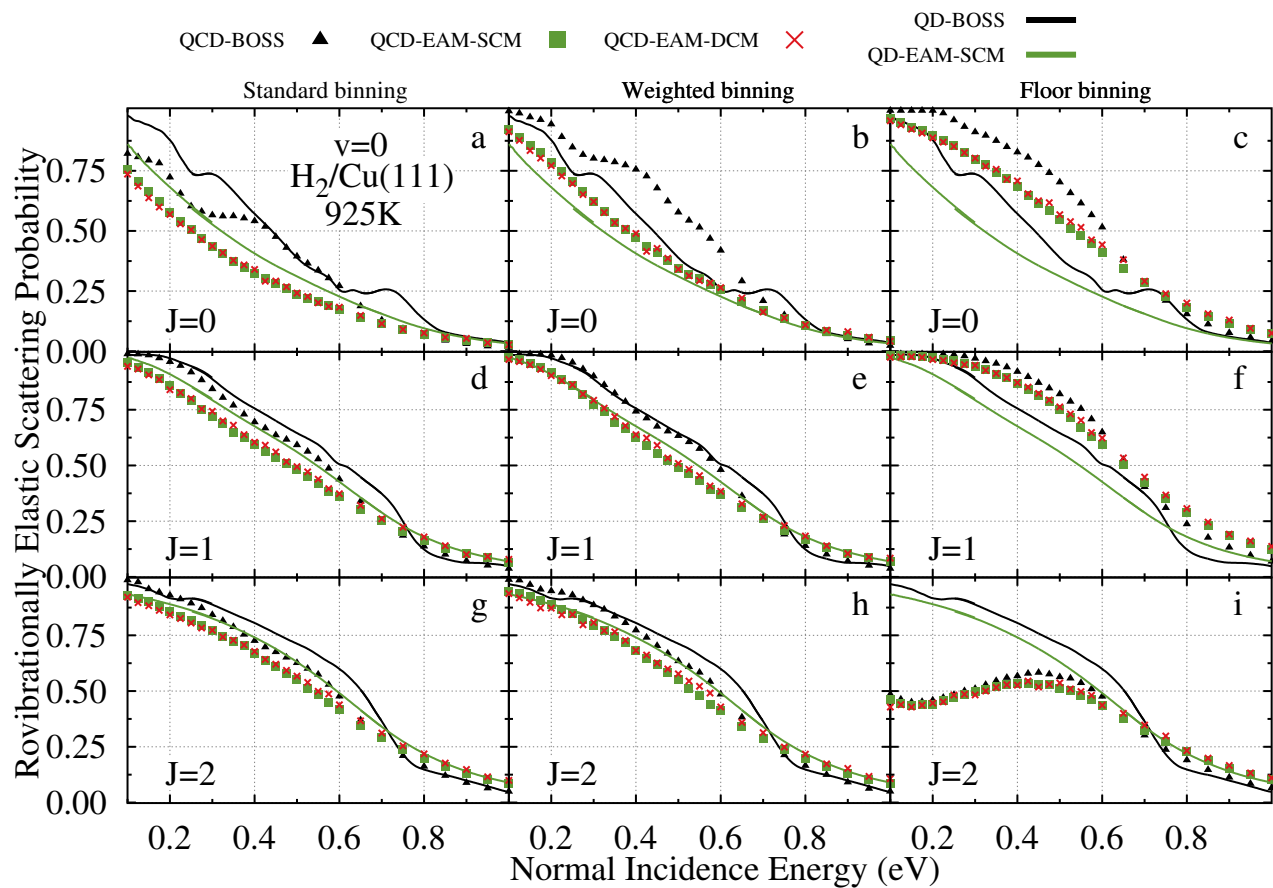


FIG. 3. Rovibrationally elastic scattering probabilities of H_2 on a $Cu(111)$ surface, obtained for the vibrational ground state ($v=0$), and three rotational states: (a-c) $J=0$; (d-f) $J=1$; and (g-i) $J=2$. Results are shown for the (a,d,g) standard, (b,e,h) weighted, and (c,f,i) floor binning methods. Included are QD- and QCD- EAM-SCM results as a green curve and green squares respectively, QD- and QCD-BOSS results as a black curve and black triangles respectively, and finally the QCD-EAM-DCM results as red crosses. A modeled surface temperature of 925K was used for the SCM and DCM.

Firstly, both Rettner *et al.* and Kaufmann *et al.* have performed beam adsorption experiments on their surfaces, which would yield accurate absolute saturation values of $A^{Rett} = 0.25$ eV and $A^{Kauf} = 0.35$ eV respectively, however due to differences in experimental conditions it is unclear if this can directly apply.¹¹ Primarily the much lower surface temperature of 120K (vs 925K here), the use of an incidence angle to vary the normal incidence energy of the molecular beam and the final rovibrational composition of this beam could all have an effect on the final results of the adsorption measurements when compared to the desorption experiments. Additional discussion on these differences can be found in Ref. 11

Next, it is suggested to use the theoretical curves to estimate an appropriate saturation value by setting the saturation value to be equal to the theoretical sticking probability at the incidence energy to which the experiment is sensitive.¹¹ This will generally yield values in the range of 0.50 to 0.60 eV. Finally, Wijzenbroek and Somers also found very good agreement between the experimental results of Hodgson *et al.* and Rettner *et al.*

when the saturation for the Hodgson results is chosen as two times that of the Rettner curve ($A^{Hodg} = 0.50$ eV).¹⁵

In Figure 5. we present these fitted experimental S-curves, and compare them to our QD- and QCD-EAM-SCM results. We have again included the initial rovibrational states of $(v,J)=(0,0)$, $(0,1)$, $(0,2)$, $(1,0)$, $(1,1)$, $(1,2)$ for (a)-(f) respectively. The uncertainty in the saturation values are shown as shaded areas for each of the curves, choosing as a minimum the results from the beam adsorption experiments when available, or $A_{Min}^{Hodg} = 0.25$ for the curve where this data is not available. As a maximum a value of $A = 0.60$ eV is chosen, as no experimental works to our knowledge has reported values higher than this. Thus the shaded areas of each color reflect the range of A parameters (see Eq. 14) each of the experimental curves could have, and visualises the uncertainty in the experimental absolute saturation values. Also included as solid lines are those curves where experimental beam adsorption results were used to obtain saturation values, when available for the experimental study, however these did not use exactly the same conditions as the desorption

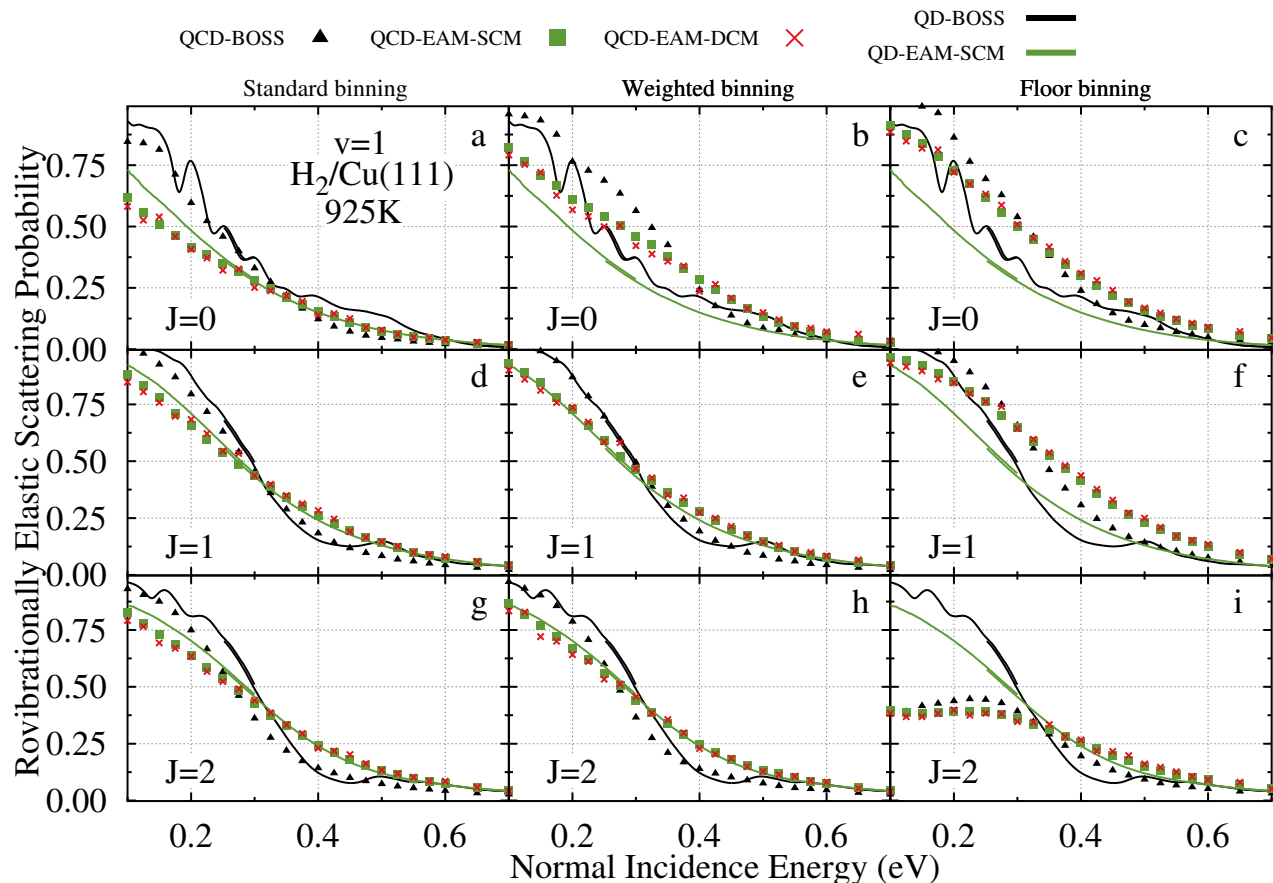


FIG. 4. Rovibrationally elastic scattering probabilities of H_2 on a $Cu(111)$ surface, obtained for the first vibrationally excited state ($v=1$), and three rotational states: (a-c) $J=0$; (d-f) $J=1$; and (g-i) $J=2$. Results are shown for the (a,d,g) standard, (b,e,h) weighted, and (c,f,i) floor binning methods. Included are QD- and QCD- EAM-SCM results as a green curve and green squares respectively, QD- and QCD-BOSS results as a black curve and black triangles respectively, and finally the QCD-EAM-DCM results as red crosses. A modeled surface temperature of 925K was used for the SCM and DCM.

experiments that were fitted originally.

Finally, the estimated saturation values for the work by Hodgson *et al.*, based on the experimental work by Rettner *et al.*, and those estimated based on the theoretical sticking probabilities are included as dashed lines in orange and red respectively. The theoretically estimated saturation values of the Kaufmann experimental fit are set to be equal to our QCD-EAM-SCM results at the highest available energy of the experimental results, as has been done in previous works.^{11,16}

Comparing the experimental results to each other, keeping in mind especially the uncertainty in saturation values, we find good agreement. Only for the rovibrational ground state do we find some disagreement for the curve onset, which can not be directly explained by this uncertainty. Interestingly the experimentally obtained curves with saturation values predicted based on the desorption experiments (shown as solid lines in blue and red) show much better agreement for the vibrationally excited states compared to the vibrational ground state. Kaufmann *et al.* similarly make this observation when

directly comparing experimentally obtained E_0 and W parameters. They believe this disagreement to be primarily caused by errors in the calibration of the older works by Rettner *et al.*, which primarily affected accurate analysis of the faster (less rovibrationally excited) molecules.¹¹

We had already previously noted the generally good agreement between the QCD- and QCD-EAM-SCM results for some of these rovibrational states, although the differences for the vibrationally excited states is also clearly present for the $v=0$, $J=1$ state, with the QD results predicting a slightly higher dissociation probability across the entire energy range investigated.

Choosing the experimental saturation values based on the theoretical sticking values in particular leads to great agreement, as can be seen when comparing the red dashed line to our theoretical results in green for every state except $v=1$, $J=0$. For this state in particular we do see excellent overlap between the QD-EAM-SCM results and the results presented by Kaufmann *et al.*, with a saturation value based on their beam adsorption exper-

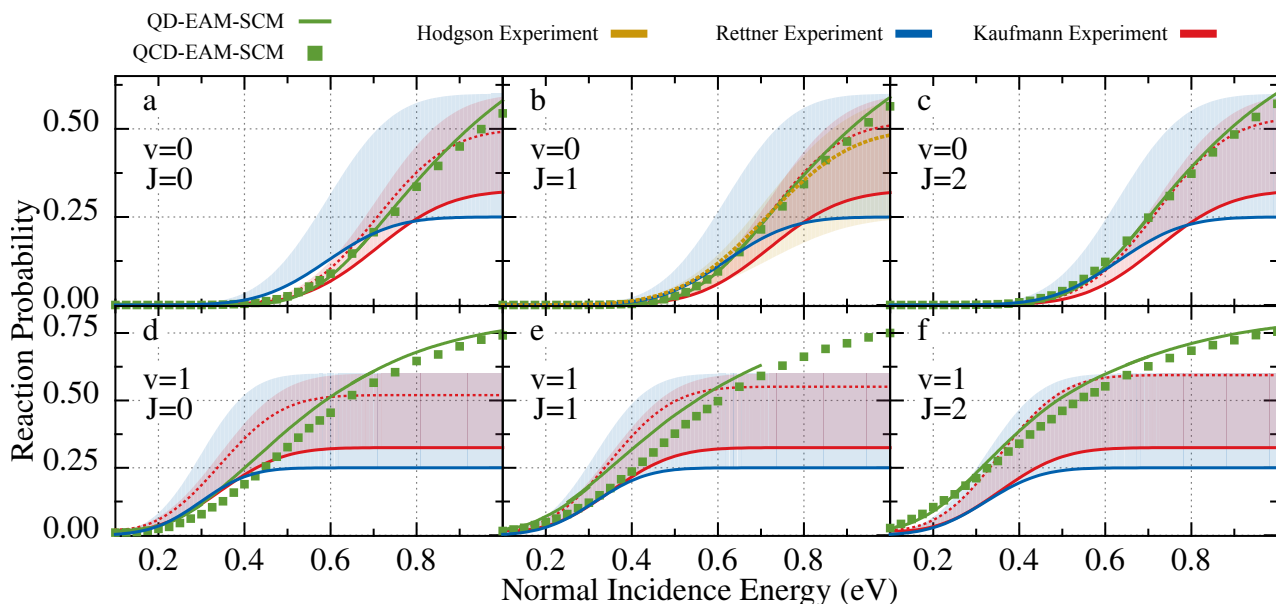


FIG. 5. Reaction probabilities obtained for six initial rovibrational states of H_2 on $\text{Cu}(111)$: (a) $v=0, J=0$; (b) $v=0, J=1$; (c) $v=0, J=2$; (d) $v=1, J=0$; (e) $v=1, J=1$; (f) $v=1, J=2$. Theoretical QD- and QCD-EAM-SCM results are shown as a green curve and green squares respectively. The experimental curves by Hodgson *et al.*,⁸ Rettner *et al.*⁷ and Kaufmann *et al.*¹¹ are included in orange, blue and red respectively, with the uncertainty in the saturation value parameters of the experimental fits shown as shaded areas. Specific experimental curves are highlighted as: (solid red / solid blue) $A_0=0.5$ eV and 0.25 eV respectively from adsorption experiments; (dashed red) saturation parameter set equal to experimental QCD-EAM-SCM value at 0.95 eV; (dashed orange) estimated $A_0 = 0.25$ value based on agreement with Rettner experiment. A (modeled) surface temperature of 925K was used for all these results.

iments. Overall agreement between the theoretical work and the experimental work is good, with the theoretical results falling well within the range of experimental saturation values we expect.

D. Logscale results

To more carefully inspect the curve onset of our dissociation results, we have plotted them again on a logarithmic scale. In Figure 6, we again present our QD- and QCD-EAM-SCM, QD- and QCD-BOSS results, as well as the QCD-EAM-DCM results, where a moving surface is included. The rovibrational states are the same as presented in Figure 1., also using the same curves and symbols.

One of the first things that can be clearly noticed is the unexpected noise, or unexpected curvature, found in the QD results of both the BOSS and EAM-SCM results. As the reaction probabilities reach very low values, noise from our QD implementation starts becoming a much more important factor of the final results. This noise can clearly be seen in the unphysical behaviour in the BOSS curves, when considering the vibrational ground state (a,c) results at low incidence energies. One of the main contributions of this noise, we believe, is the error inherent to the SPO method in Eq. 9, which is inherent to the step-wise integration method of the SPO and

scales with Δt^3 . Thus smaller and smaller time-steps are needed to accurately describe reaction probabilities ($P \lesssim 10^{-3}$), much lower than those we have used for our calculations (see supplementary material). Reducing the time-step by a factor 10 should reduce the expected noise due to the SPO propagation by as much as a factor of 10^3 while only increasing the computational load by a factor of 10. However, other factors and parameters of the WPs would also start to play a more dominant role in the final error we observe. We consider the additional computational time needed to properly sample enough distorted surfaces for the SCM while also reducing this time-step to be unfeasible for this study, although we believe it could be an important topic for later work.

Those results we expect to be either partially, or perhaps fully, dominated by this noise we have included using a different curve color, with a lighter shade of either black for BOSS or green for the EAM-SCM results. However, an upturn of reaction probability does seem to appear for very low incidence energies which is not visible at all for our QCD results. Recent work by Dutta *et al.* report a similar upturn for the $\text{D}_2/\text{Cu}(111)$ system, investigated with the same SRP48 BOSS PES and QD implementation, but using the effective Hartree potential method to include surface temperature effects.²⁹ They believe this could be attributed to vibrational degrees of freedom, due to a modeled elevated surface temperature, which could match the slow channel as reported by Kauf-

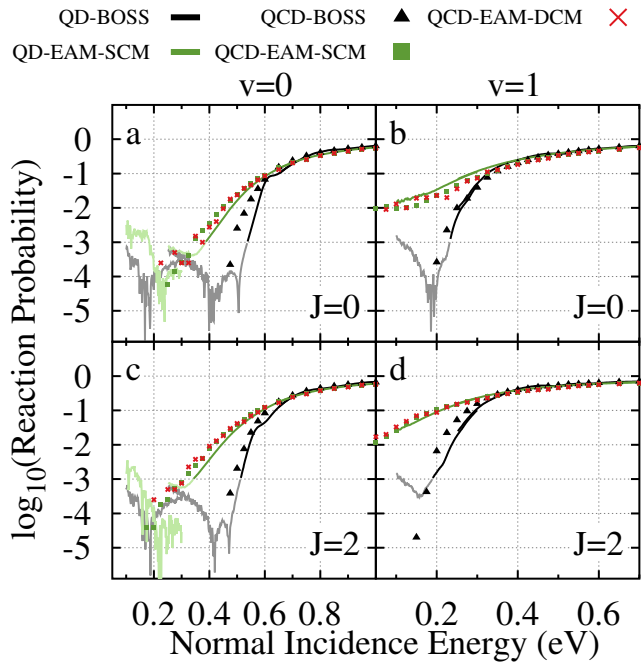


FIG. 6. Reaction probabilities obtained for four initial rovibrational states of H_2 on Cu(111): (a) $v=0$, $J=0$; (b) $v=1$, $J=0$; (c) $v=0$, $J=2$; (d) $v=1$, $J=2$, with the reaction probabilities on a logarithmic scale. Theoretical QD- and QCD-EAM-SCM results are shown as a green curve and green squares respectively, and QD- and QCD-BOSS results as a black curve and black triangles. QD results where noise is expected to play a major role are shown as a lighter shade curve. QCD-EAM-DCM results are included as red crosses. A modeled surface temperature of 925K was used for all the SCM and DCM results.

mann *et al.*¹¹ This EfHP work, however, uses the same SPO propagation method and is thus also expected to exhibit errors of a similar magnitude as our work, which is covered in both works. Furthermore, we also observe an upturn for the ideal lattice BOSS model, which suggests something more than purely attributing this to surface vibrational DoF. Thus, this would be a prime target for further studies, using more carefully crafted WPs and employing much smaller time-steps in the SPO to investigate the very low incidence energy regions of our H_2 on Cu(111) system, because at the moment we also do not yet have theoretical explanations of why such an upturn should be present in our BOSS results.

For the higher incidence energies, where the error in our QD results is expected to be small, we do still see great agreement with the QCD results, both for the BOSS and EAM-SCM results. The much more rapid drop in reactivity as the incidence energy decreases seen in the BOSS results, when compared to the EAM-SCM results, matches the observation of increased curve broadness when higher surface temperatures are taken into account.^{15,16,62} For both PESs and every initial rovibrational state, the QCD calculations yield slightly higher

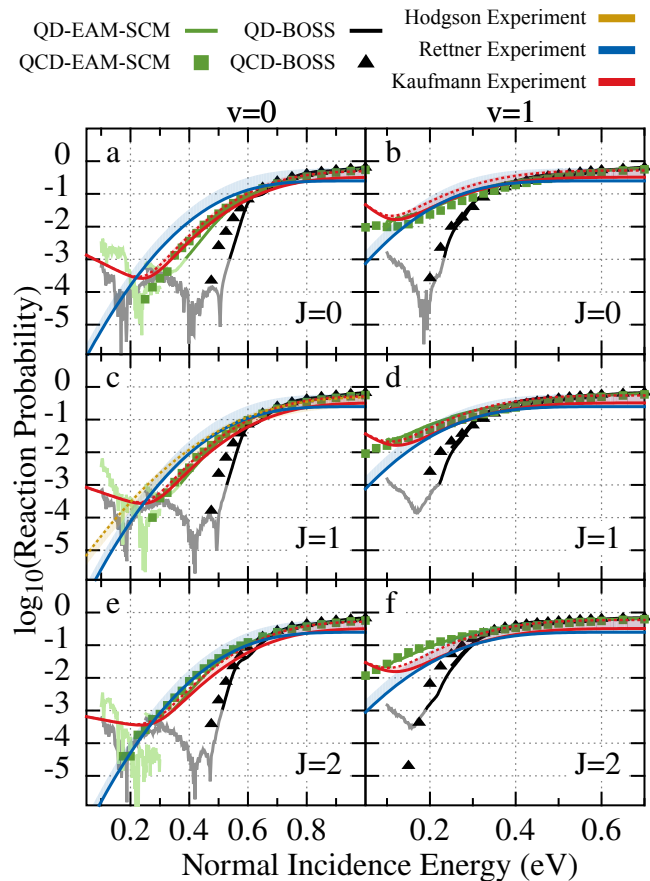


FIG. 7. Reaction probabilities obtained for six initial rovibrational states of H_2 on Cu(111): (a) $v=0$, $J=0$; (b) $v=1$, $J=0$; (c) $v=0$, $J=1$; (d) $v=1$, $J=1$; (e) $v=0$, $J=2$; (f) $v=1$, $J=2$, with the reaction probabilities on a logarithmic scale. Theoretical QD- and QCD-EAM-SCM results are shown as a green curve and green squares respectively, and QD- and QCD-BOSS results as a black curve and black triangles. QD results where noise is expected to play a major role are shown as a lighter shade. The experimental curves by Hodgson *et al.*,⁸ Rettner *et al.*⁷ and Kaufmann *et al.*¹¹ are included in orange, blue and red respectively, with the uncertainty in the saturation value parameters of the experimental fits shown as shaded areas. Additional curves are shown the same as in Figure 5. A (modeled) surface temperature of 925K was used for all these results.

reaction probabilities, except for the EAM-SCM results of the $v=1$, $J=0$ state, where this relation is inverted. This confirms again the quality of the EAM-SCM implementation at a QD level, and shows we can accurately include the thermal surface effects into our QD simulations, even at lower energies. Furthermore, the EAM-DCM results almost perfectly match those of the EAM-SCM, again showing the validity of a static surface approximation for our specific system, and the minimal amount of effect energy exchange has for this dissociation reaction.

Finally in Figure 7. we will compare the curve onset of

our theoretical dissociation curves to those found in the experimental works we consider. The same states and results are presented as we had shown in Figure 5., but now we also included the QD- and QCD-BOSS results. Again we have used shaded areas to mark the uncertainty in the absolute experimental A values, which appears as a small static shift on the logarithmic scale. Furthermore, the contribution of the slow reaction channel reported by Kaufmann *et al.* now also become much more apparent at low incidence energies. Neither the work by Rettner *et al.* nor the work by Hodgson *et al.* reported observing this channel in their work.

Overlap between our QD- and QCD-EAM-SCM curves and the experimental results of Kaufmann *et al.* is in general excellent even for very low reaction probabilities, with the biggest differences found for the rovibrational ground state and the highest excited state we included ($v=1, J=2$). However, a clear difference is found for the QCD-EAM-SCM results at very low incidence energies, as they do not predict any kind of slow channel. While the QD-EAM-SCM, and even the QD-BOSS, results do appear to predict an increase in reactivity at these very low energies, it is, at the moment, still unclear if this an actual physical effect or an artefact introduced by our QD approach (or the CRP BOSS PES). Nevertheless, an upturn has been observed both in this study, and by Dutta *et al.* using a similar QD approach, but with a different method of including surface temperature effects, but also using the same BOSS PES and the same V_{coup} of the SCM to construct the effective time-dependent Hartree potential.²⁹ Again it should be emphasized that this work, as well as the work of Dutta *et al.*, is still as of yet inconclusive given the expected magnitude of errors in the QD simulations for these low probabilities. Fascinating though is the suggested presence of the apparent signal even in our older BOSS calculations, and as of yet we lack an explanation for it (predominantly because of the errors in the approximations we have to make in the QD). Thus, a more thorough theoretical investigation of this upturn, both with the SCM and the EfHP method, would be a very important topic for further studies. However, these will be computationally challenging computations, as reducing the time-step by a factor of 10 will increase the computational costs by a factor of 10. Especially when also considering this for $T_s=925\text{K}$. One then has to perform these 10 times more expensive calculations for at least 100 individual surface configurations, making such a study truly state-of-the-art and currently out of the scope for this paper.

IV. CONCLUSION

We investigated the quality of the EAM-SCM approach to including all relevant surface temperature effects, at both a quantum dynamical and quasi-classical level, using the dissociative chemisorption of H_2 on $\text{Cu}(111)$ (at a surface temperature of 925K) as a model system. We

computed both reaction and rovibrationally elastic scattering probabilities, and compared those to values obtained from the dynamic surface EAM-DCM and to H_2 sticking curves from experimental studies. We also investigated several simple binning methods, to validate the agreement between the QCD probabilities, and those obtained using rigorous quantum dynamics simulations. Our BOSS PES was constructed by Nattino *et al.*⁴³ using the CRP, with datapoints obtained from DFT using SRP48 functional, while the SCM distorted surface corrections were described by the effective three-body SCM coupling potential as published by Spiering *et al.*²⁰ The thermally distorted surface configurations for the SCM were obtained from a highly accurate EAM potential using molecular dynamics, as published previously by Smits and Somers.

While previous work had already shown the QCD- and QD-EAM-SCM dissociation probabilities agreed well for the rovibrational ground state, we demonstrated this also holds true for several initially rovibrationally excited states. The three different binning methods we investigated did not appear to significantly affect these probabilities, although weighted binning did slightly reduce the predicted QCD reaction probabilities, which reduced agreement with the QD curves.

Much bigger effects were found for the rovibrational elastic scattering, where either this weighted binning or our standard binning demonstrated better agreement with the curves obtained from QD simulations, for both the EAM-SCM and the BOSS approach. The final method of binning, floor binning, was found to greatly overestimate rovibrationally elastic scattering probabilities for the lower energy rovibrational states, but then greatly underestimated the same probabilities for those states that had more rovibrational energy available and had allowed scattering states with similar energies. As it only affected the determination of the final state of scattered molecules, the floor binning did not change reaction probabilities compared to our standard binning method. Overall, we believe both the standard and weighted binning performed equally well, and as such could both be of interest for further studies.

Taking into account the uncertainty in absolute experimental saturation values, due to the nature of the direct inversion of desorption results used in the experimental method, we also found excellent agreement between our (QD-)EAM-SCM results and the experimental curves published by Rettner *et al.*,⁷ Hodgson *et al.*⁸ and Kaufmann *et al.*¹¹ Even for the curve onset, where reaction is best plotted on a logarithmic scale, we see good overlap with our theoretical results. At very low incidence energies, our QD results even indicate a small upturn in reaction similar to those found by Kaufmann *et al.*, also found by Dutta *et al.* using their EfHP method and the same QD code,²⁹ but not before been reported in any other theoretical works. However, great care should be taken when interpreting our QD results in this regime, as the very low probabilities involved enables the noise inherent

to the SPO method to become an important contribution to our final results. More carefully constructed wave packets, using a much smaller time-step to minimise the error when propagating, would allow for a more thorough analysis of this slow channel using QD simulations.

In general, this work has shown that the EAM-SCM approach to including surface temperature effects into quasi-classical and quantum dynamical simulations works well for the H₂ on Cu(111) system, at least at a surface temperature of 925K. Comparisons to the dynamic surface EAM-DCM results further validate the sudden approximation made in the model, while comparisons to experimental results show that the model holds both for the rovibrational ground state, as well as several rovibrationally excited states. However, several other observables found in literature, such as rotational/vibrational efficacies and rovibrationally inelastic scattering probabilities, have not yet been verified and thus are an interesting subject for further study. Equally, the noise introduced by the SPO method made it difficult to convincingly show the slow channel of the H₂/Cu(111) system can be observed at a theoretical level using the EAM-SCM and thus would be an excellent target for further work, both using our SCM and the EfHP method by Dutta *et al.*

SUPPLEMENTARY MATERIAL

See the supplementary material for the computational details of the TDWP quantum dynamics simulations of H₂ dissociation on a Cu(111) surface.

ACKNOWLEDGEMENTS

The authors thank Professor Dr. G.-J. Kroes and NWO-EW for providing the computational resources needed to obtain these results and the rest of the theoretical chemistry group for their feedback on this project.

AUTHOR DECLARATIONS

Conflict of Interest

The authors have no conflicts to disclose.

DATA AVAILABILITY

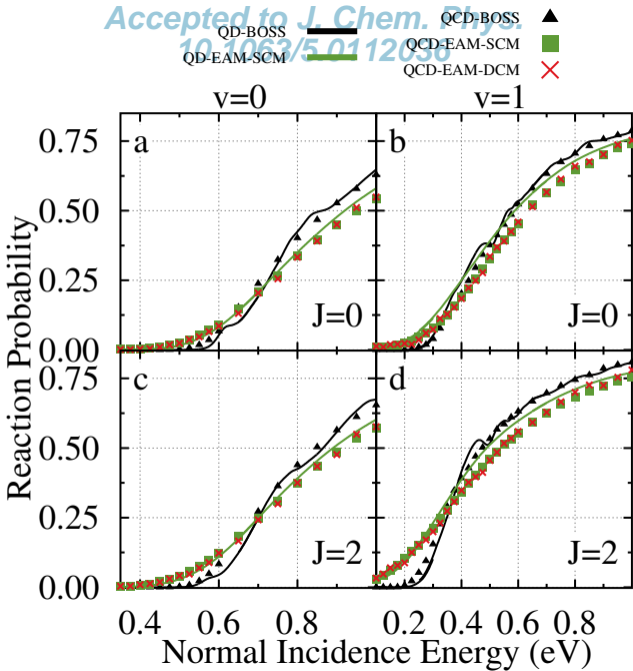
The data that support the findings of this study are available from the research group's public repository at <https://pubs.tc.lic.leidenuniv.nl/>.

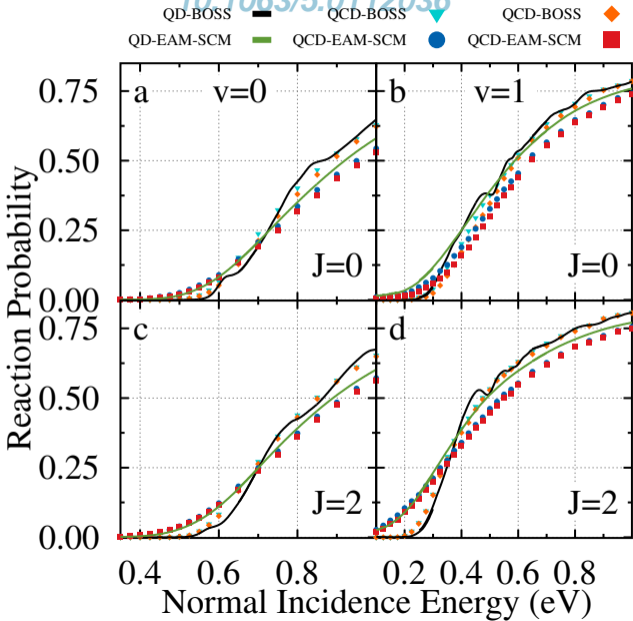
REFERENCES

- I. Chorkendorff, *Concepts of Modern Catalysis and Kinetics* (Wiley-VCH, Weinheim, 2003).
- C. Smith, A. K. Hill, and L. Torrente-Murciano, "Current and future role of Haber–Bosch ammonia in a carbon-free energy landscape," *Energy & Environmental Science* **13**, 331–344 (2020).
- C. T. Campbell, "The Degree of Rate Control: A Powerful Tool for Catalysis Research," *ACS Catalysis* **7**, 2770–2779 (2017).
- G.-J. Kroes, "Computational approaches to dissociative chemisorption on metals: towards chemical accuracy," *Physical Chemistry Chemical Physics* **23**, 8962–9048 (2021).
- H. F. Berger, M. Leisch, A. Winkler, and K. D. Rendulic, "A search for vibrational contributions to the activated adsorption of H₂ on copper," *Chemical Physics Letters* **175**, 425–428 (1990).
- H. A. Michelsen, C. T. Rettner, D. J. Auerbach, and R. N. Zare, "Effect of rotation on the translational and vibrational energy dependence of the dissociative adsorption of D₂ on Cu(111)," *The Journal of Chemical Physics* **98**, 8294–8307 (1993).
- C. T. Rettner, H. A. Michelsen, and D. J. Auerbach, "Quantum-state-specific dynamics of the dissociative adsorption and associative desorption of H₂ at a Cu(111) surface," *The Journal of Chemical Physics* **102**, 4625–4641 (1995).
- A. Hodgson, P. Samson, A. Wight, and C. Cottrell, "Rotational Excitation and Vibrational Relaxation of H₂ Scattered from Cu(111)," *Physical Review Letters* **78**, 963–966 (1997).
- H. Hou, S. J. Gulding, C. T. Rettner, A. M. Wodtke, and D. J. Auerbach, "The Stereodynamics of a Gas-Surface Reaction," *Science* **277**, 80–82 (1997), publisher: American Association for the Advancement of Science Section: Report.
- M. J. Murphy and A. Hodgson, "Adsorption and desorption dynamics of H₂ and D₂ on Cu(111): The role of surface temperature and evidence for corrugation of the dissociation barrier," *The Journal of Chemical Physics* **108**, 4199–4211 (1998).
- S. Kaufmann, Q. Shuai, D. J. Auerbach, D. Schwarzer, and A. M. Wodtke, "Associative desorption of hydrogen isotopologues from copper surfaces: Characterization of two reaction mechanisms," *The Journal of Chemical Physics* **148**, 194703 (2018).
- H. Chadwick, M. F. Somers, A. C. Stewart, Y. Alkoby, T. J. D. Carter, D. Butkovicova, and G. Alexandrowicz, "Stopping molecular rotation using coherent ultra-low-energy magnetic manipulations," *Nature Communications* **13**, 2287 (2022).
- C. Díaz, E. Pijper, R. A. Olsen, H. F. Busnengo, D. J. Auerbach, and G. J. Kroes, "Chemically accurate simulation of a prototypical surface reaction: H₂ dissociation on Cu(111)," *Science (New York, N.Y.)* **326**, 832–834 (2009).
- C. Díaz, R. A. Olsen, D. J. Auerbach, and G. J. Kroes, "Six-dimensional dynamics study of reactive and non reactive scattering of H₂ from Cu(111) using a chemically accurate potential energy surface," *Physical Chemistry Chemical Physics* **12**, 6499–6519 (2010).
- M. Wijzenbroek and M. F. Somers, "Static surface temperature effects on the dissociation of H₂ and D₂ on Cu(111)," *The Journal of Chemical Physics* **137**, 054703 (2012).
- F. Nattino, A. Genova, M. Guijt, A. S. Muzas, C. Díaz, D. J. Auerbach, and G.-J. Kroes, "Dissociation and recombination of D₂ on Cu(111): ab initio molecular dynamics calculations and improved analysis of desorption experiments," *The Journal of Chemical Physics* **141**, 124705 (2014).
- M. Bonfanti, M. F. Somers, C. Díaz, H. F. Busnengo, and G.-J. Kroes, "7D Quantum Dynamics of H₂ Scattering from Cu(111): The Accuracy of the Phonon Sudden Approximation," *Zeitschrift für Physikalische Chemie*, 130617035227002 (2013).
- A. Mondal, M. Wijzenbroek, M. Bonfanti, C. Díaz, and G.-J. Kroes, "Thermal Lattice Expansion Effect on Reactive Scattering of H₂ from Cu(111) at T_s = 925 K," *The Journal of Physical Chemistry A* **117**, 8770–8781 (2013).
- G.-J. Kroes, J. I. Juaristi, and M. Alducin, "Vibrational Excitation of H₂ Scattering from Cu(111): Effects of Surface Temper-

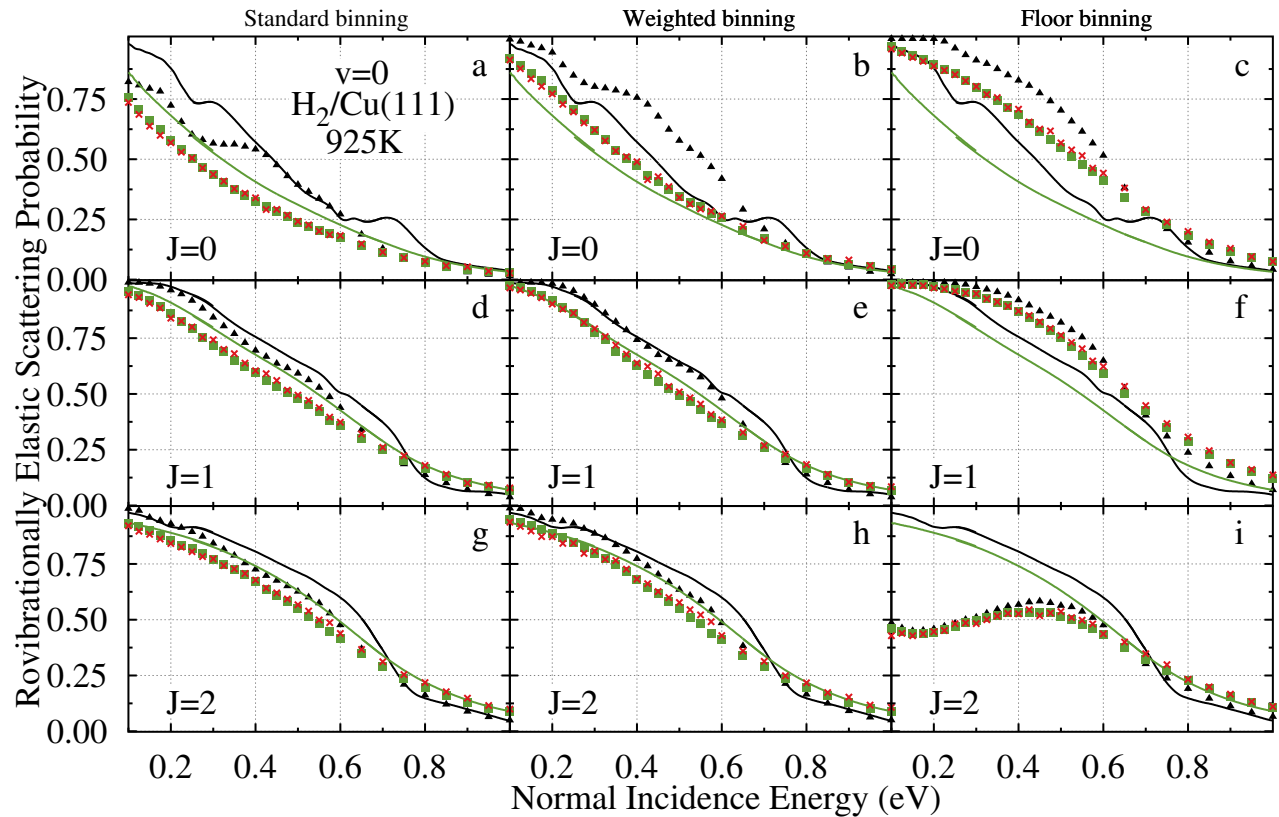
- ature and of Allowing Energy Exchange with the Surface,” *The Journal of Physical Chemistry C* **121**, 13617–13633 (2017).
- ²⁰P. Spiering, M. Wijzenbroek, and M. F. Somers, “An improved static corrugation model,” *The Journal of Chemical Physics* **149**, 234702 (2018).
- ²¹L. Zhu, Y. Zhang, L. Zhang, X. Zhou, and B. Jiang, “Unified and transferable description of dynamics of H₂ dissociative adsorption on multiple copper surfaces *via* machine learning,” *Physical Chemistry Chemical Physics* **22**, 13958–13964 (2020).
- ²²O. Galparsoro, S. Kaufmann, D. J. Auerbach, A. Kandratsenka, and A. M. Wodtke, “First principles rates for surface chemistry employing exact transition state theory: Application to recombinative desorption of hydrogen from Cu(111),” *Physical Chemistry Chemical Physics* **22**, 17532–17539 (2020).
- ²³B. Smits and M. F. Somers, “Beyond the static corrugation model: Dynamic surfaces with the embedded atom method,” *The Journal of Chemical Physics* **154**, 074710 (2021).
- ²⁴E. W. F. Smeets and G.-J. Kroes, “Designing new SRP density functionals including non-local vdW-DF2 correlation for H₂ + Cu(111) and their transferability to H₂ + Ag(111), Au(111) and Pt(111),” *Physical Chemistry Chemical Physics* **23**, 7875–7901 (2021).
- ²⁵E. W. F. Smeets and G.-J. Kroes, “Performance of Made Simple Meta-GGA Functionals with rVV10 Nonlocal Correlation for H₂ + Cu(111), D₂ + Ag(111), H₂ + Au(111), and D₂ + Pt(111),” *The Journal of Physical Chemistry C* **125**, 8993–9010 (2021).
- ²⁶B. Smits, L. G. B. Litjens, and M. F. Somers, “Accurate description of the quantum dynamical surface temperature effects on the dissociative chemisorption of H₂ from Cu(111),” *The Journal of Chemical Physics* **156**, 214706 (2022).
- ²⁷H. Chadwick, Y. Alkoby, J. T. Cantin, D. Lindebaum, O. Godsi, T. Maniv, and G. Alexandrowicz, “Molecular spin echoes; multiple magnetic coherences in molecule surface scattering experiments,” *Physical Chemistry Chemical Physics* **23**, 7673–7681 (2021).
- ²⁸J. Dutta, S. Mandal, S. Adhikari, P. Spiering, J. Meyer, and M. F. Somers, “Effect of surface temperature on quantum dynamics of H₂ on Cu(111) using a chemically accurate potential energy surface,” *The Journal of Chemical Physics* **154**, 104103 (2021).
- ²⁹J. Dutta, K. Naskar, S. Adhikari, P. Spiering, J. Meyer, and M. F. Somers, “Effect of surface temperature on quantum dynamics of D₂ on Cu(111) using a chemically accurate potential energy surface,” (2022), To Be Submitted.
- ³⁰A. K. Tiwari, S. Nave, and B. Jackson, “The temperature dependence of methane dissociation on Ni(111) and Pt(111): Mixed quantum-classical studies of the lattice response,” *The Journal of Chemical Physics* **132**, 134702 (2010).
- ³¹H. Guo, A. Farjammia, and B. Jackson, “Effects of Lattice Motion on Dissociative Chemisorption: Toward a Rigorous Comparison of Theory with Molecular Beam Experiments,” *The Journal of Physical Chemistry Letters* **7**, 4576–4584 (2016).
- ³²B. Jackson, “Quantum studies of methane-metal inelastic diffraction and trapping: The variation with molecular orientation and phonon coupling,” *Chemical Physics* **559**, 111516 (2022).
- ³³G. J. Kroes, M. Wijzenbroek, and J. R. Manson, “Possible effect of static surface disorder on diffractive scattering of H₂ from Ru(0001): Comparison between theory and experiment,” *The Journal of Chemical Physics* **147**, 244705 (2017).
- ³⁴Y. Xiao, W. Dong, and H. F. Busnengo, “Reactive force fields for surface chemical reactions: A case study with hydrogen dissociation on Pd surfaces,” *The Journal of Chemical Physics* **132**, 014704 (2010).
- ³⁵A. Lozano, X. J. Shen, R. Moiraghi, W. Dong, and H. F. Busnengo, “Cutting a chemical bond with demon’s scissors: Mode- and bond-selective reactivity of methane on metal surfaces,” *Surface Science Reactivity Concepts at Surfaces: Coupling Theory with Experiment*, **640**, 25–35 (2015).
- ³⁶G. N. Seminara, I. F. Peludhero, W. Dong, A. E. Martínez, and H. F. Busnengo, “Molecular Dynamics Study of Molecular and Dissociative Adsorption Using System-Specific Force Fields Based on Ab Initio Calculations: CO/Cu(110) and CH₄/Pt(110),” *Topics in Catalysis* **62**, 1044–1052 (2019).
- ³⁷I. R. Craig and D. E. Manolopoulos, “Quantum statistics and classical mechanics: Real time correlation functions from ring polymer molecular dynamics,” *The Journal of Chemical Physics* **121**, 3368–3373 (2004).
- ³⁸Y. V. Suleimanov, F. J. Aoiz, and H. Guo, “Chemical Reaction Rate Coefficients from Ring Polymer Molecular Dynamics: Theory and Practical Applications,” *The Journal of Physical Chemistry A* **120**, 8488–8502 (2016).
- ³⁹J. Behler, “First Principles Neural Network Potentials for Reactive Simulations of Large Molecular and Condensed Systems,” *Angewandte Chemie International Edition* **56**, 12828–12840 (2017).
- ⁴⁰N. Artrith and J. Behler, “High-dimensional neural network potentials for metal surfaces: A prototype study for copper,” *Physical Review B* **85**, 045439 (2012).
- ⁴¹Q. Lin, L. Zhang, Y. Zhang, and B. Jiang, “Searching Configurations in Uncertainty Space: Active Learning of High-Dimensional Neural Network Reactive Potentials,” *Journal of Chemical Theory and Computation* **17**, 2691–2701 (2021).
- ⁴²H. F. Busnengo, A. Salin, and W. Dong, “Representation of the 6D potential energy surface for a diatomic molecule near a solid surface,” *The Journal of Chemical Physics* **112**, 7641–7651 (2000).
- ⁴³F. Nattino, C. Díaz, B. Jackson, and G.-J. Kroes, “Effect of Surface Motion on the Rotational Quadrupole Alignment Parameter of D₂ Reacting on Cu(111),” *Physical Review Letters* **108**, 236104 (2012).
- ⁴⁴G.-J. Kroes and C. Díaz, “Quantum and classical dynamics of reactive scattering of H₂ from metal surfaces,” *Chemical Society Reviews* **45**, 3658–3700 (2016).
- ⁴⁵H. W. Sheng, M. J. Kramer, A. Cadien, T. Fujita, and M. W. Chen, “Highly optimized embedded-atom-method potentials for fourteen fcc metals,” *Physical Review B* **83**, 134118 (2011).
- ⁴⁶P. Spiering and J. Meyer, “Testing Electronic Friction Models: Vibrational De-excitation in Scattering of H₂ and D₂ from Cu(111),” *The Journal of Physical Chemistry Letters* **9**, 1803–1808 (2018).
- ⁴⁷L. Sementa, M. Wijzenbroek, B. J. van Kolck, M. F. Somers, A. Al-Halabi, H. F. Busnengo, R. A. Olsen, G. J. Kroes, M. Rutkowski, C. Thewes, N. F. Kleimeier, and H. Zacharias, “Reactive scattering of H₂ from Cu(100): Comparison of dynamics calculations based on the specific reaction parameter approach to density functional theory with experiment,” *The Journal of Chemical Physics* **138**, 044708 (2013).
- ⁴⁸E. W. F. Smeets, G. Füchsel, and G.-J. Kroes, “Quantum Dynamics of Dissociative Chemisorption of H₂ on the Stepped Cu(211) Surface,” *The Journal of Physical Chemistry C* **123**, 23049–23063 (2019).
- ⁴⁹G. Füchsel, T. Klamroth, S. Monturet, and P. Saalfrank, “Dissipative dynamics within the electronic friction approach: The femtosecond laser desorption of H₂/D₂ from Ru(0001),” *Physical Chemistry Chemical Physics* **13**, 8659 (2011).
- ⁵⁰R. J. Maurer, B. Jiang, H. Guo, and J. C. Tully, “Mode Specific Electronic Friction in Dissociative Chemisorption on Metal Surfaces: H₂ on Ag(111),” *Physical Review Letters* **118**, 256001 (2017).
- ⁵¹P. Spiering, K. Shakouri, J. Behler, G.-J. Kroes, and J. Meyer, “Orbital-Dependent Electronic Friction Significantly Affects the Description of Reactive Scattering of N₂ from Ru(0001),” *The Journal of Physical Chemistry Letters* **10**, 2957–2962 (2019).
- ⁵²M. D. Feit, J. A. Fleck, and A. Steiger, “Solution of the Schrödinger equation by a spectral method,” *Journal of Computational Physics* **47**, 412–433 (1982).
- ⁵³G.-J. Kroes and M. F. Somers, “Six-dimensional dynamics of dissociative chemisorption of H₂ on metal surfaces,” *Journal of Theoretical and Computational Chemistry* **04**, 493–581 (2005).
- ⁵⁴A. Vibok and G. G. Balint-Kurti, “Parametrization of complex absorbing potentials for time-dependent quantum dynamics,”

- The Journal of Physical Chemistry **96**, 8712–8719 (1992).
- ⁵⁵G. G. Balint-Kurti, R. N. Dixon, and C. C. Marston, “Grid methods for solving the Schrödinger equation and time dependent quantum dynamics of molecular photofragmentation and reactive scattering processes,” *International Reviews in Physical Chemistry* **11**, 317–344 (1992).
- ⁵⁶B. Jiang and H. Guo, “Six-dimensional quantum dynamics for dissociative chemisorption of H₂ and D₂ on Ag(111) on a permutation invariant potential energy surface,” *Phys. Chem. Chem. Phys.* **16**, 24704–24715 (2014).
- ⁵⁷G.-J. Kroes, “Six-dimensional quantum dynamics of dissociative chemisorption of H₂ on metal surfaces,” *Progress in Surface Science* **60**, 1–85 (1999).
- ⁵⁸C. C. Marston and G. G. Balint-Kurti, “The Fourier grid Hamiltonian method for bound state eigenvalues and eigenfunctions,” *The Journal of Chemical Physics* **91**, 3571–3576 (1989).
- ⁵⁹R. Bulirsch and J. Stoer, “Numerical treatment of ordinary differential equations by extrapolation methods,” *Numerische Mathematik* **8**, 1–13 (1966).
- ⁶⁰A. Rodríguez-Fernández, L. Bonnet, C. Crespos, P. Larrégaray, and R. Díez Muiño, “When Classical Trajectories Get to Quantum Accuracy: The Scattering of H₂ on Pd(111),” *The Journal of Physical Chemistry Letters* **10**, 7629–7635 (2019).
- ⁶¹A. Rodríguez-Fernández, L. Bonnet, C. Crespos, P. Larrégaray, and R. Díez Muiño, “When classical trajectories get to quantum accuracy: II. The scattering of rotationally excited H₂ on Pd(111),” *Physical Chemistry Chemical Physics* **22**, 22805–22814 (2020).
- ⁶²R. D. Muino and H. F. Busnengo, eds., *Dynamics of Gas-Surface Interactions: Atomic-level Understanding of Scattering Processes at Surfaces*, Springer Series in Surface Sciences (Springer-Verlag, Berlin Heidelberg, 2013).





QCD-BOSS \blacktriangle QCD-EAM-SCM \blacksquare QCD-EAM-DCM \times QD-BOSS ---
 QD-EAM-SCM ---



QCD-BOSS

▲

QCD-EAM-SCM

■

QCD-EAM-DCM

×

QD-BOSS

—

QD-EAM-SCM

—

Standard binning

Weighted binning

Floor binning

Rovibrationally Elastic Scattering Probability

 $v=1$
 $H_2/Cu(111)$
925K

J=0

J=0

J=0

J=1

J=1

J=1

J=2

J=2

J=2

a

b

c

d

e

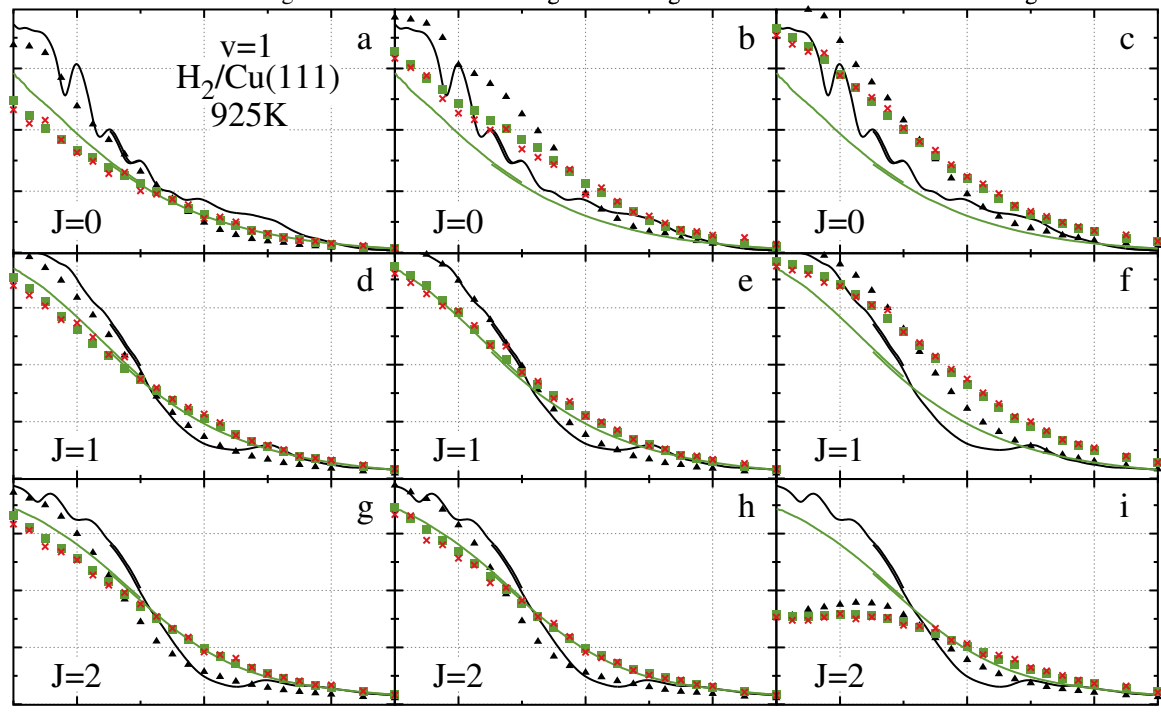
f

g

h

i

Normal Incidence Energy (eV)



QD-EAM-SCM  Hodgson Experiment  Rettner Experiment  Kaufmann Experiment 
QCD-EAM-SCM 

